Additive Manufacturing 23 (2018) 132–139

Contents lists available at ScienceDirect

Additive Manufacturing

journal homepage: www.elsevier.com/locate/addma

Full Length Article

Investigation of process-structure-property relationships in polymer extrusion based additive manufacturing through in situ high speed imaging and thermal conductivity measurements

Darshan Ravoori, Lorenzo Alba, Hardikkumar Prajapati, Ankur Jain*

Mechanical and Aerospace Engineering Department, University of Texas at Arlington, Arlington, TX, USA

ARTICLE INFO

Keywords:
Additive manufacturing
Polymer extrusion
Thermal conductivity
High speed imaging
Process-structure-property relationships

ABSTRACT

Additive manufacturing has gained significant research attention due to multiple advantages over traditional manufacturing technologies. A fundamental understanding of the relationships between process parameters, microstructure and functional properties of built parts is critical for optimizing the additive manufacturing process and building parts with desired properties. This is also critical for a multi-functional part where the process needs to be optimized with respect to disparate performance requirements such as mechanical strength and thermal conductivity. This paper presents *in situ* high speed imaging and build-direction thermal conductivity measurements of polymer extrusion based additively manufactured parts in order to understand the effect of process parameters such as raster speed, infill percentage and layer height on build-direction thermal conductivity. Measurements of thermal conductivity using a one-dimensional heat flux method are correlated with *in situ* process images obtained from a high speed camera as well as cross section images of the built part. Results indicate strong dependence of build-direction thermal conductivity on raster speed, layer thickness and infill percentage, which is corroborated by high speed imaging of the printing process at different values of these process parameters. Key trade-offs between process throughput and thermal properties are also identified. In addition to enhancing our fundamental understanding of polymer extrusion based additive manufacturing and its influence on thermal properties of built parts, results presented here may facilitate process optimization towards parts with desired thermal and multi-functional properties.

1. Introduction

Additive Manufacturing (AM) [1–3] offers several advantages compared to traditional manufacturing methods, and therefore, is currently being investigated for a wide variety of applications [4–7]. Broadly, AM techniques can be classified into two categories – metal-based AM involving processes such as Selective Laser Sintering (SLS) [8,9], or polymer extrusion based AM [10,11]. These techniques offer increased design flexibility, capability of producing nearly-arbitrary shapes and the possibility of tailored properties of printed parts [1,2]. In polymer extrusion processes, a polymer filament is heated to above the glass transition temperature and extruded on to a platform [10]. The extruded polymer lines – often referred to as roads – merge into neighboring lines as they cool, thereby imparting mechanical strength and rigidity to the built part. Multiple layers of such polymer lines are dispensed on top of previously built layers, and the shape of the part is controlled by spatially selective deposition of polymer filament in each layer. A large amount of literature exists on understanding and optimizing the polymer extrusion based AM process [10,12–14], including the various sub-processes such as filament heating, extrusion, deposition, as well as post-process treatment.

The merging of adjacent polymer roads into each other plays a key role in determining the microstructure, and hence the overall properties and performance of the built part [10]. This is a dynamic process that is likely to depend on a number of process parameters, such as raster speed, extrusion temperature, *etc.*, as well as the properties of the polymer material such as glass transition temperature, temperature-dependent viscosity, surface tension, *etc.*, some of which have been investigated in the past [12–14]. Multiple highly coupled physical processes occur during the merging process, including cooling and glass transition, surface tension driven flow and integration of polymer strands between adjacent roads [12]. Understanding and optimizing these processes and their interactions is critical for obtaining desired microstructure, and ultimately for obtaining properties of interest in the

* Corresponding author at: 500W First St, Rm 211, Arlington, TX, USA.
E-mail address: jaina@uta.edu (A. Jain).

https://doi.org/10.1016/j.addma.2018.07.011
Received 2 March 2018; Received in revised form 9 July 2018; Accepted 24 July 2018
Available online 25 July 2018

built part. Several papers have carried out theoretical and numerical modeling of the filament extrusion and deposition process, including theoretical models [15,16] and numerical simulations [17,18] to predict thermal profiles following deposition. While these studies provide much needed theoretical insight into the microscale processes underlying polymer extrusion AM, there is also a need for correlating these processes with the properties of the built part, for example, by connecting these properties with the microstructure resulting from various process parameters. *In situ* visualization of the AM process, particularly the dispensing and merging of adjacent roads, and post-process property measurement could play a key role in developing these correlations.

A number of studies have investigated the effect of various process parameters on the ultimate properties of the built part [19–23]. Most of these studies have focused on mechanical and structural properties such as mechanical strength, Young's modulus, *etc.* Anisotropic mechanical properties have been reported as a function of print speed and raster orientation [22]. Tensile strength has been shown to correlate with layer height [24]. Raster angle of 0° and 90° has been shown to result in maximum and minimum tensile strength respectively. The latter is shown to fail in transverse load because the load is taken up by the bonding between fibers and not the fibers themselves [19]. Tensile strength of criss-cross rastering has been shown to fall in between the two extremes [19]. In comparison to the considerable literature on mechanical properties, there is relatively lesser work available on thermal properties of built parts and their relationship with microstructure and process parameters. These properties, such as thermal conductivity govern the nature of heat flow through the part [25], and therefore, are critical for understanding the performance of the part in an engineering application where heat generation and heat flow may be important considerations. Similar to mechanical properties such as mechanical strength, it is reasonable to expect that thermal conductivity will be influenced by the microstructure of the built part. For example, the extent of adhesion between adjacent roads may influence the amount of heat flow, and hence the value of the thermal conductivity. Specifically, poor adhesion resulting from incorrectly designed process parameters is expected to lead to insufficient heat flow, and hence poor thermal conductivity.

Clearly, there is a need to identify optimum process parameters that result in parts with desired thermal properties. The relationships between process, microstructure and properties have not been sufficiently studied in the context of thermal performance of built parts. The effect of sintering on filament bonding has been studied [16]. However, this is a post-printing process, whereas it would be more effective to understand and optimize parameters related to the printing process itself, in order to result in desired thermal properties.

Further, several applications call for multifunctional parts that must perform both thermal and structural function. For example, structural parts often need to provide thermal insulation as well. In such a case, it is critical to optimize the process parameters and microstructure in order to obtain a balance between mechanical strength and thermal conductivity, along with weight considerations. Addressing this complicated problem requires an integrated approach involving both microscale visualization to understand microstructure, as well as part-scale measurement of thermal properties to fully understand the impact of process parameters on thermal properties. Such an approach, while entailing multiple experimental challenges is expected to enhance the fundamental understanding of polymer extrusion based AM, as well as result in optimized build strategies for specific parts.

This paper presents high speed, microscale visualization of polymer extrusion based additive manufacturing integrated with thermal property measurements. High speed imaging of the process is carried out for different values of key process parameters such as raster speed, layer height, *etc.* These images are used to determine the dependence of microstructure on process parameters. The variation of thermal properties of the built part on process parameters is characterized through measurement of thermal conductivity in the build direction based on a one-dimensional heat flux method. Results indicate strong dependence of thermal conductivity on raster speed and layer thickness, which is corroborated by high speed imaging of the printing process at different values of these process parameters. The extent of inter-layer adhesion expected from imaging experiments correlates well with thermal conductivity measurements of built parts. These results are expected to extend the fundamental understanding of microscale processes underlying polymer based AM and their relationships with the properties of the eventual part, particularly in the context of thermal properties. Process optimization carried out based on these results may be instrumental in designing and building parts with desired, multi-functional properties.

2. Experiments

Experiments are carried out to identify the dependence of build direction thermal conductivity, k_z on various process parameters including extruder print speed, layer height and infill percentage. *In situ* visualization of the rastering process is carried out using high speed imaging, which helps identify the key microstructural features of the built part and correlates these with process parameters. In addition, thermal conductivity measurements are carried out on the built parts in order to understand the effect of process parameters and microstructure on the resulting thermal properties of the part.

2.1. Fabrication of test samples

Fabrication of samples is carried out on a polymer extrusion based, open source 3D printer using 1.75 mm diameter black polylactic acid (PLA) material. The process parameters studied in this work include raster speed, infill percentage and layer height. Raster speed is varied in the 1000–18000 mm/min range, while infill percentage is varied between 50% and 95%. Layer height in the 0.2–2.5 mm range is investigated. Print temperature is held constant at 215 °C, and a 0.4 mm diameter nozzle is used in all experiments. Two samples of thicknesses 4 mm and 8 mm are printed for thermal conductivity measurement as outlined in Section 2.3. Each sample has a size of 40 mm by 40 mm. Geometry for each sample is modeled in Solidworks and exported to Simplify3D software for slicing. The G-code generated in this manner is directed to the 3D printer for printing with specified build process parameters.

2.2. In situ high speed imaging

In situ high speed imaging of the polymer printing process is carried out in order to understand the process of adhesion between adjacent lines, and correlate the microstructure of printed lines with process parameters on one hand, and thermal properties of the printed part on the other. A FASTEC Imaging IL5SM4 high speed camera is arranged at a sideways angle in order to view the rastering process. In conjunction, a Navitar 12 V 150 W high intensity fiber optic illuminator source is used for improving the image quality. Videos of the rastering process are recorded at a rate of 120 frames per second, with minimum 3μs shutter time and pixel size of 5 μm by 5 μm. Fig. 1(a) shows a picture of the experimental setup, showing the 3D printer, as well as the high speed camera and illumination used for video capture.

The *in-situ* high speed imaging during the rastering process is supplemented with post-processing cross-section imaging of printed samples. In order to preserve the internal microstructure of parts during the cutting process, samples are cut carefully using liquid nitrogen. Four small notches are first made on the four edges of the sample of interest. The sample is then immersed in liquid nitrogen for two minutes, and an impact load in applied on one of the notches. Cross sections of cut samples are imaged using a 10 megapixel AMScope microscope digital camera in conjunction with an AmScope 3X stereomicroscope.

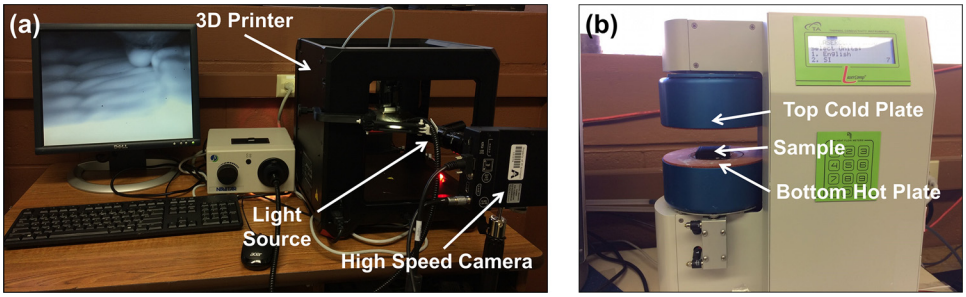

Fig. 1. (a) Picture of experimental setup showing the 3D printer, high speed camera and high intensity light source; (b) Picture of thermal conductivity measurement setup.

2.3. Thermal conductivity measurements

Thermal conductivity of the built parts is measured in the build direction by applying a temperature difference across a test sample and measuring the resulting heat flux using the Fox50 thermal conductivity measurement instrument. Fig. 1(b) shows a picture of the experimental setup for thermal conductivity measurement. A picture of the representative samples of two different thicknesses (4 mm and 8 mm) is shown in Fig. 2.

In order to account for interfacial thermal contact resistance between the sample and the instrument during thermal conductivity measurements, separate measurements are carried out on samples of two different thicknesses, and the difference between the total thermal resistances between the two samples is used to determine the thermal conductivity of the material.

The measured total thermal resistance, which is the ratio of temperature difference and heat flux, comprises contributions from thermal resistance of the sample material and the two interfaces between the sample and instrument plates.

$$R_T = 2R_c + R_m \tag{1}$$

The material thermal resistance R_m in Eq. (1) is given by L/k, where L and k are the thickness and thermal conductivity of the sample respectively. Assuming that interfacial thermal resistance, R_c is the same for two samples of thicknesses L_1 and L_2, the thermal conductivity of the sample material may be determined from the measured total thermal resistance R_{T1} and R_{T2} for the two samples by eliminating R_c as follows [26].

$$k = \frac{L_1 - L_2}{R_{T1} - R_{T2}} \tag{2}$$

A guard wall is used around the sample during measurements for minimizing lateral heat loss. The instrument is calibrated by measuring thermal conductivity of standard pyrex samples of two different thicknesses using this method, which is found to result in very close agreement with the standard value (1.11 W/mK *vs.* 1.09 W/mK). Measurements are carried out on multiple sets of samples printed with different process parameters. Variation of thermal conductivity with infill percentage, layer height and raster speed is analyzed and correlated with imaging of the rastering process through the high speed camera.

3. Results and discussion

3.1. Progression of the polymer rastering process

Fig. 3(a) through (d) show images of the rastering process captured at 1 s intervals during the printing process at 6000 mm/min speed, 100% infill and 0.4 mm layer height. In reference to these images, the polymer lines are printed from bottom to top of the image, and the extruder moves towards the left after printing each line. The structure of deposited lines is clearly seen in these images, which appear to adhere well with their neighboring lines. The underlying layer of lines deposited orthogonally prior to the present layer, as well as the nozzle head are also visible in these images. Fig. 3(a) through (d) represent successive images of the process captured for a baseline case. The effect of changing various parameters is investigated next.

3.2. Effect of changing infill percentage

Experiments are carried out at multiple values of the infill density between 50% and 95% while holding the raster speed and layer height constant at 6000 mm/min and 0.4 mm respectively. Images from these experiments are shown in Fig. 4(a) through (d) for four different infill percentage values. These images clearly show a significant effect of the infill density on the microstructure. As expected, the polymer lines are far apart and disperse at 50% infill, and get increasingly closer to each other at larger infill percentages. As a result, a greater infill percentage is expected to result in higher thermal conductivity due to improved adhesion as shown in Fig. 4. This is investigated through measurement of thermal conductivity of these samples. The measured thermal conductivity, plotted in Fig. 5 clearly increases with increasing infill

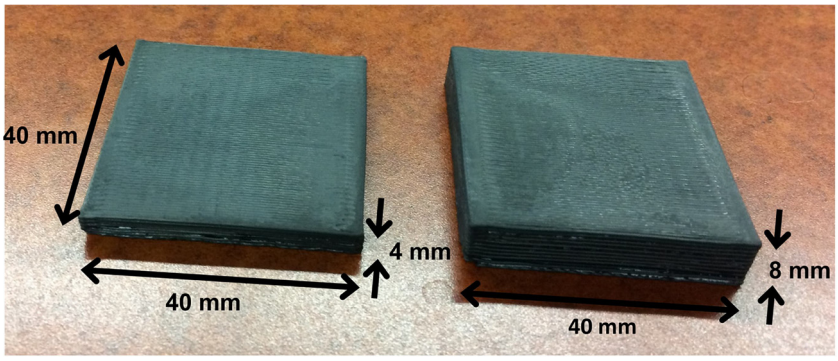

Fig. 2. Pictures of 4 mm and 8 mm thickness samples with 40 mm by 40 mm sides printed for thermal conductivity measurements.

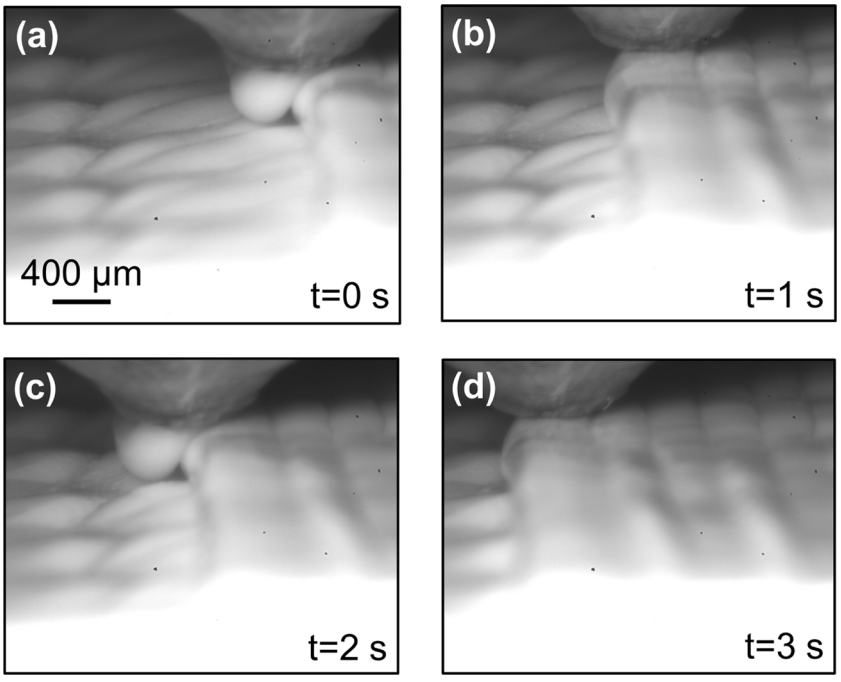

Fig. 3. Images of the baseline 3D printing process at 6000 mm/min raster speed, 100% infill and 0.4 mm layer height. Parts (a) through (d) shows images at 1 s intervals captured through the high speed camera.

percentage. This variation is found to fit well by a linear curve. Fig. 5 also shows cross section images of printed samples obtained with a microscope digital camera for the highest and lowest infill percentage cases. The cross-section image for 50% infill indicates significant gaps between lines, which is consistent both with the corresponding *in situ* rastering image in Fig. 4(a) as well as the low value of the measured thermal conductivity. Similar consistency is observed between the cross section for the 95% infill, which shows tight packing of lines, and corresponding *in situ* image and thermal conductivity measurements. These data and images clearly indicate that infill percentage plays a key role in determining thermal conductivity through its influence on the microstructure. Note that each thermal conductivity plotted in Fig. 5, and in all subsequent figures, represents an average of measurements taken on three samples printed with the same set of parameters. A tight fit is found among these three data in each case, with the worst-case deviation of less than 3%.

The effective thermal conductivity of the sample may be modeled as a combination of the thermal conductivities of the filament material and air gap. While the exact nature of how these thermal conductivities combine may not be known, lower and upper limits for the combined

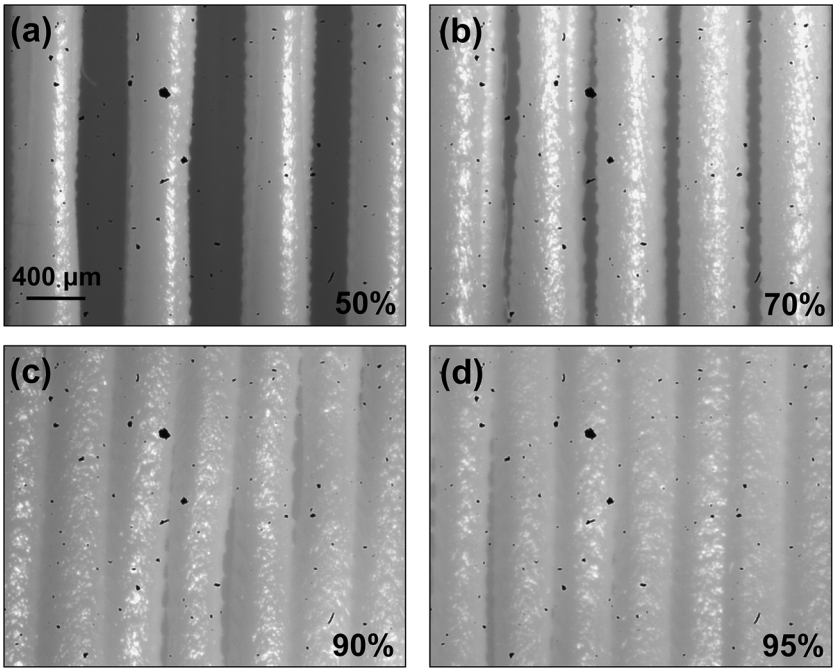

Fig. 4. Images of the 3D printing process at different infill density values. Parts (a) through (d) show images at the end of the process for 50%, 70%, 90% and 95% infill density respectively at raster speed and layer height of 6000 mm/min and 0.4 mm respectively.

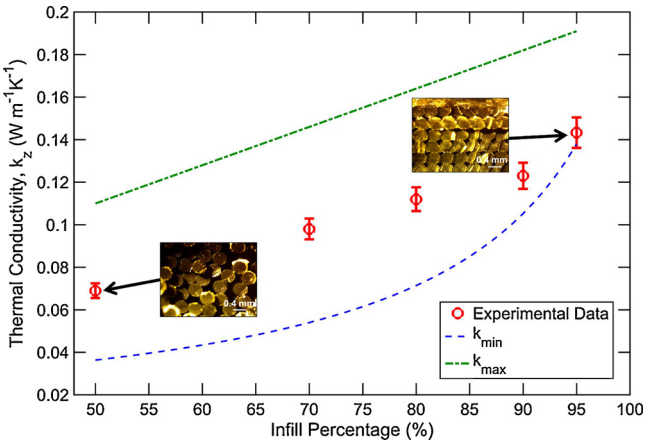

Fig. 5. Plot showing the variation of measured build direction thermal conductivity with infill density. Cross section images of samples for 50% and 95% infill clearly show the impact of infill on the microstructure of the printed part. Theoretically calculated upper and lower limits based on series/parallel combination of thermal resistances are also shown for comparison with experimental data.

thermal conductivities may be estimated from series and parallel combinations of the two thermal resistances based on the infill percentage as follows:

$$\frac{1}{k_{min}} = \frac{\varphi}{k_{air}} + \frac{1-\varphi}{k_{filament}} \tag{3}$$

and

$$k_{max} = \varphi k_{air} + (1-\varphi)k_{filament} \tag{4}$$

where φ is the infill percentage.

k_{min} and k_{max} are plotted in Fig. 5 as functions of φ for comparison with experimental data. Fig. 5 shows that experimentally measured thermal conductivity at each infill percentage lies between the theoretically predicted upper and lower limits. This provides a validation of the experimental measurements.

3.3. Effect of raster speed

High speed imaging and post-printing thermal conductivity measurements are carried out at four different raster speeds for a 100% infill and 0.4 mm layer height. Fig. 6 shows high speed images of the printing process at four different times for each raster speed. These images show the effect of raster speed on the microstructure. Slow raster speed offers more time for heat transfer to the underlying and adjacent filaments, which causes these lines to remain at elevated temperatures for greater time, and therefore merge with each other effectively. This is expected to result in improved thermal conductivity. On the other hand, the merging process may remain incomplete if the raster speed is too high, and heat transfer between filaments is not complete, resulting in lower thermal conductivity. In order to further investigate this, thermal conductivity of printed parts is measured for various raster speeds. Fig. 7 shows greater thermal conductivity at lower raster speeds, which confirms the hypothesis above about the effect of raster speed on filament merging. Cross-section images of samples printed at different raster speeds, shown in Fig. 7 are in general consistent with *in situ* imaging and corresponding thermal conductivity measurements. A comparison of these cross section images at different raster speeds indicates better merging between filaments and greater infill at lower raster speeds, which corroborates well with the measurement of higher thermal conductivity at lower raster speeds.

3.4. Effect of layer height

The effect of layer height on thermal conductivity is investigated next. In these experiments, raster speed and infill percentage are fixed at 6000 mm/min and 100% respectively, while layer height is varied between 0.2 mm and 2.5 mm. Measurements summarized in Fig. 8 show that thermal conductivity increases with increasing layer height. This is because for the same overall sample size, a greater layer height results in lower number of layers, and hence reduced number of interfaces between layers. This results in diminished contribution of inter-layer thermal contact resistance, and hence, increased build-direction thermal conductivity. This is consistent with recent measurements and modeling that have indicated a dominant role of the thermal contact resistance in build-direction thermal conductivity of the sample [27]. The reduced number of interfaces between layers is clear from the cross-section images shown in Fig. 8. These measurements and images confirm the dominant role of inter-layer thermal contact resistance on thermal properties.

3.5. Effect of raster orientation

It is of practical relevance to understand how raster orientation impacts thermal conductivity. Raster orientation is a commonly available setting in most polymer AM platforms. In most cases, the raster orientation can be set to toggle between two angles from one layer to the next. Samples are printed for four different raster orientations − 0°/0°, 0°/90°, +20°/−20° and +45°/−45°. In the first case, raster lines in successive layers are all oriented in the same direction, while in the second case, raster lines are orthogonal to each other. In the other cases, raster lines criss-cross each other at the specified angles. Thermal conductivity of each sample is measured using the methods discussed above. Fig. 9 shows measured thermal conductivity values for these cases, along with cross section images. These measurements indicate some dependence of thermal conductivity on raster orientation. Specifically, it is found that thermal conductivity is largest for 0°/0° and 0°/90° cases. For cases where the raster lines in successive layers are at other, non-orthogonal angles (+20°/−20° and +45°/−45°), a lower value of thermal conductivity is measured. This likely occurs due to reduced contact between successive layers due to the non-orthogonal angle.

3.6. Discussion

The experimental measurements and imaging data discussed in subsections above establish a correlation between thermal conductivity of built parts and various process parameters. These data can provide critical input for determining the right process parameters for obtaining specific thermal properties of interest in the built part. Further, these data also indicate the possibility of obtaining spatially varying thermal properties by smartly changing process parameters in different parts of the build. For example, it may be possible to dynamically reduce raster speed within the feasible parameter space for manufacturability in a specific portion of the part being built in order to obtain higher thermal conductivity only in that portion. Such a capability may result in integrated parts with unique functionality for multiple applications.

Further, several applications call for multifunctional parts, for example those that must serve both thermal and structural function. In such a case, optimization of process parameters is important from both thermal and structural perspectives. Results presented in this work, in conjunction with past reports on mechanical properties, may help drive such an optimization. In cases where high thermal conductivity is required in addition to good mechanical strength, the variations of both objectives as functions of process parameters are in general aligned with each other. For example, reducing raster speed may increase both mechanical strength and thermal conductivity. However, in other applications, there may exist a conflict between the two objectives. For

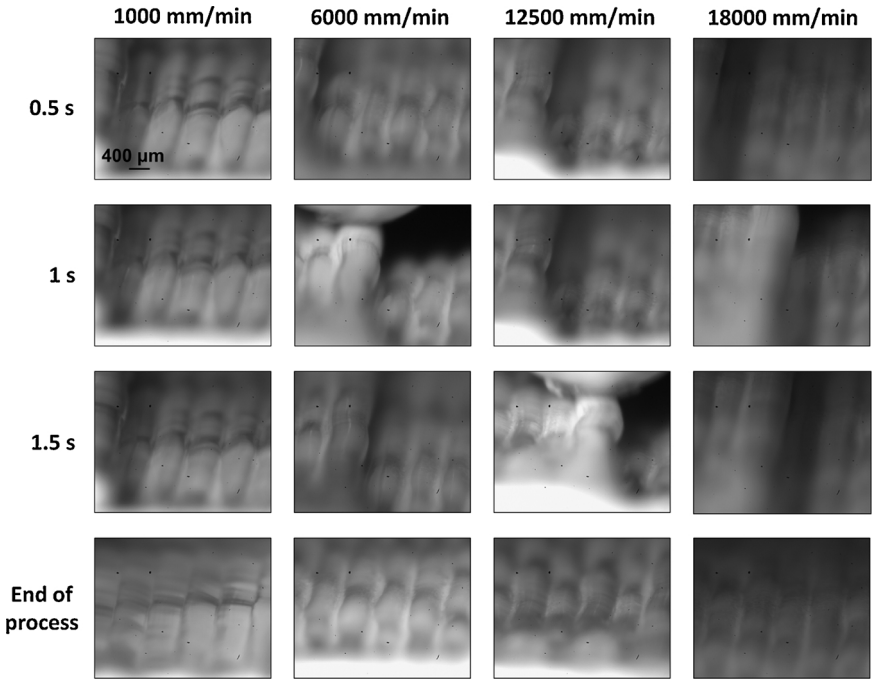

Fig. 6. Images of the 3D printing process at different times for four different raster speeds. The change is microstructure with raster speed at the end of process results in different thermal conductivity values for different raster speeds.

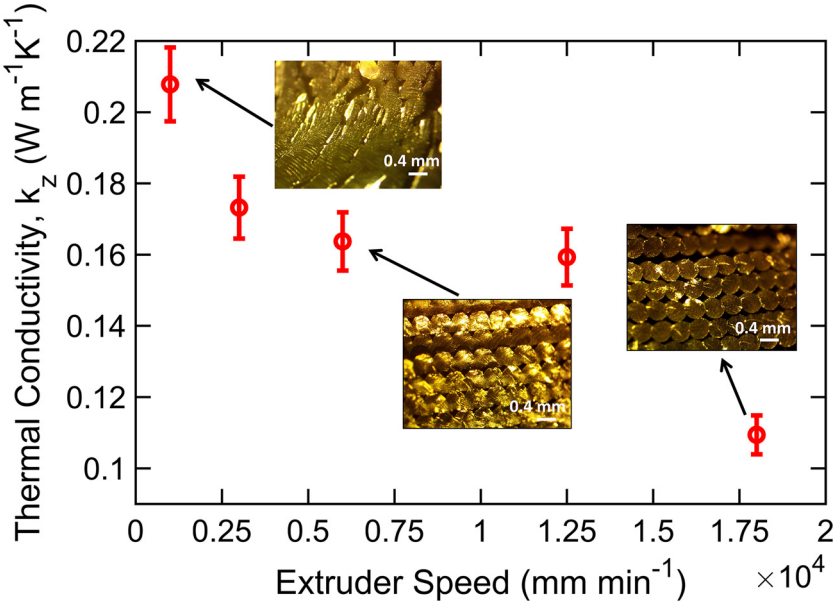

Fig. 7. Plot showing the variation of build direction thermal conductivity with raster speed. Cross section images of samples for two cases are also shown. The measured variation agrees well with observations of the microstructure through *in situ* high speed imaging and cross-section imaging.

example, in applications where a structural part must also provide thermal insulation, reducing the infill percentage will improve thermal insulation, as shown in this work, but will also likely result in reduced strength. A careful co-optimization of process parameters within the feasible parameter space based on results from this work may be important for resolving such trade-offs.

Finally, there also exist trade-offs between desired thermal properties and system-level process performance that this work helps resolve. For example, while reducing the raster speed has been shown to increase thermal conductivity, which may be desirable for certain applications, it will also severely reduce throughput. Results presented here may also be useful for understanding and resolving such trade-offs.

4. Conclusions

This work combines *in situ* high speed imaging of the polymer extrusion based additive manufacturing process with post-print, build-direction thermal conductivity measurements to investigate the relationships between process parameters, microstructure and eventual properties of the built part. Given the significant design flexibility enabled by additive manufacturing, a thorough understanding of these relationships is critical in order to maximize the benefit of additive manufacturing within the feasible design space. This becomes even more important in the case of multifunctional parts where more than one properties of the built part must be balanced with other considerations such as processing time, weight, *etc.*, all within the given

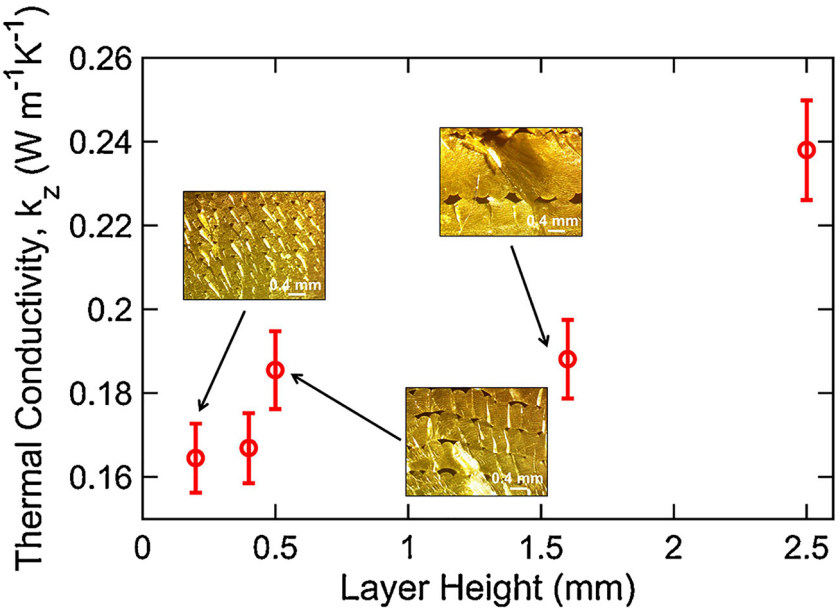

Fig. 8. Plot showing the variation of build direction thermal conductivity with layer height for the same overall sample size. The increase in thermal conductivity with increasing layer height clearly indicates the key role of interfacial thermal contact resistance in determining thermal conductivity in the build direction.

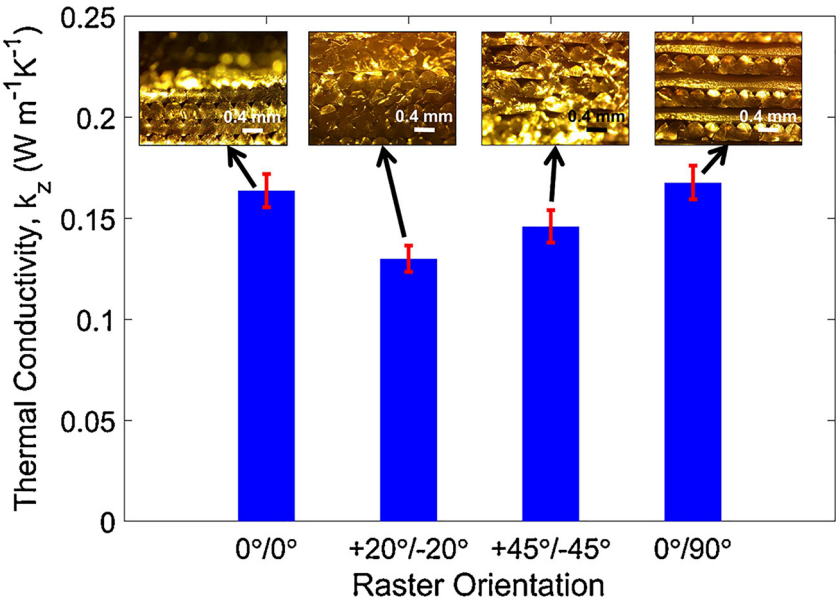

Fig. 9. Measured build-direction thermal conductivity as a function of raster orientation.

feasible parametric space of manufacturability. The present work enables such optimization by developing relationships between process parameters and thermal properties of interest in a variety of applications. Results indicate strong dependence of build direction thermal conductivity on various process parameters such as raster speed, layer height, *etc.* In addition to improving the fundamental understanding of polymer extrusion based additive manufacturing process, this work may also enable the printing of parts with novel thermal transport properties.

References

[1] J.P. Kruth, M.C. Leu, T. Nakagawa, Progress in additive manufacturing and rapid prototyping, CIRP Anal. Manuf. Technol. 2 (1998) 525–540.
[2] K.V. Wong, A. Hernandez, A review of additive manufacturing, ISRN Mech. Eng. 1 (2012) 1–10.
[3] W.E. Frazier, Metal additive manufacturing: a review, J. Mater. Eng. Perform. 23 (2014) 1917–1928.
[4] N. Guo, M.C. Leu, Additive manufacturing: technology, applications and research needs, Front. Mech. Eng. 8 (2013) 215–243.
[5] H.J. Timothy, H.L.A. Ola, Overview of current additive manufacturing technologies and selected applications, Sci. Prog. 95 (2012) 255–282.
[6] O. Ivanova, C. Williams, T. Campbell, Additive manufacturing (AM) and nanotechnology: promises and challenges, Rapid Prototyp. J. 19 (2013) 353–364.
[7] V. Petrovic, J.V.H. Gonzalez, O.J. Ferrando, J.D. Gordillo, J.R.B. Puchades, L.P. Griñan, Additive layered manufacturing: sectors of industrial application shown through case studies, Int. J. Prod. Res. 49 (2011) 061–1079.
[8] N.K. Tolochko, M.K. Arshinov, A.V. Gusarov, V.I. Titov, T. Laoui, L. Froyen, Mechanisms of selective laser sintering and heat transfer in Ti powder, Rapid Prototyp. J. 9 (2003) 314–326.
[9] J.P. Kruth, X. Wang, T. Laoui, L. Froyen, Lasers and materials in selective laser sintering, Assem. Autom. 23 (2003) 357–371.
[10] F. Ning, W. Cong, J. Qiu, J. Wei, S. Wang, Additive manufacturing of carbon fiber reinforced thermoplastic composites using fused deposition modeling, Compos. Part B 80 (2015) 369–378.
[11] S. Upcraft, R. Fletcher, The rapid prototyping technologies, Assem. Autom. 23 (2003) 318–330.
[12] K. Thrimurthulu, P.M. Pandey, N.V. Reddy, Optimum part deposition orientation in

fused deposition modeling, Int. J. Mach. Tools Manuf. 44 (2004) 585–594.
[13] J.W. Stansbury, M.J. Idacavagec, 3D printing with polymers: challenges among expanding options and opportunities, Dent. Mater. 32 (2016) 54–64.
[14] B.H. Lee, J. Abdullah, Z.A. Khan, Optimization of rapid prototyping parameters for production of flexible ABS object, J. Mater. Process. Technol. 169 (2005) 54–61.
[15] C. Bellehumeur, L. Li, Q. Sun, P. Gu, Modeling of bond formation between polymer filaments in the fused deposition modeling process, J. Manuf. Process. 6 (2004) 170–178.
[16] Q. Sun, G.M. Rizvi, C.T. Bellehumeur, P. Gu, Effect of processing conditions on the bonding quality of FDM polymer filaments, J. Manuf. Process. 14 (2008) 72–80.
[17] M. Nikzada, S.H. Masooda, I. Sbarskia, A. Grothb, A study of melt flow analysis of an ABS-Iron composite in fused deposition modelling process, Tsinghua Sci. Technol. 14 (2009) 29–37.
[18] H. Bikas, P. Stavropoulos, G. Chryssolouris, Additive manufacturing methods and modelling approaches: a critical review, Int. J. Adv. Manuf. Technol. 83 (2016) 389–405.
[19] S. Ahn, M. Montero, D. Odell, S. Roundy, P.K. Wright, Anisotropic material properties of fused deposition modeling ABS, Rapid Prototyp. J. 8 (2002) 248–257.
[20] R. Anitha, S. Arunachalam, P. Radhakrishnan, Critical parameters influencing the quality of prototypes in fused deposition modelling, J. Mater. Process. Technol. 118 (2001) 385–388.
[21] A.K. Sood, R.K. Ohdar, S.S. Mahapatra, Parametric appraisal of mechanical property of fused deposition modelling processed parts, Mater. Des. 31 (2010) 287–295.
[22] F. Ning, W. Cong, Y. Hu, H. Wang, Additive manufacturing of carbon fiber-reinforced plastic composites using fused deposition modeling: effects of process parameters on tensile properties, J. Compos. Mater. 51 (2016) 451–462.
[23] A.K. Sooda, R.K. Ohdar, S.S. Mahapatra, Experimental investigation and empirical modelling of FDM process for compressive strength improvement, J. Adv. Res. 3 (2012) 81–90.
[24] B.M. Tymrak, M. Kreiger, J.M. Pearce, Mechanical properties of components fabricated with open-source 3-D printers under realistic environmental conditions, Mater. Des. 58 (2014) 242–246.
[25] F.P. Incropera, D.P. DeWitt, T.L. Bergman, A.S. Levine, Introduction to Heat Transfer, 5th ed., John Wiley & Sons, 2006.
[26] V. Vishwakarma, C. Waghela, A. Jain, Measurement of out-of-plane thermal conductivity of substrates for flexible electronics and displays, Microelectron. Eng. 142 (July) (2015) 36–39.
[27] H. Prajapati, D. Ravoori, R. Woods, A. Jain, Measurement of anisotropic thermal conductivity and inter-layer thermal contact resistance in polymer fused deposition modeling (FDM), Addit. Manuf. 21 (May) (2018) 84–90.